Supplementary Figure 1

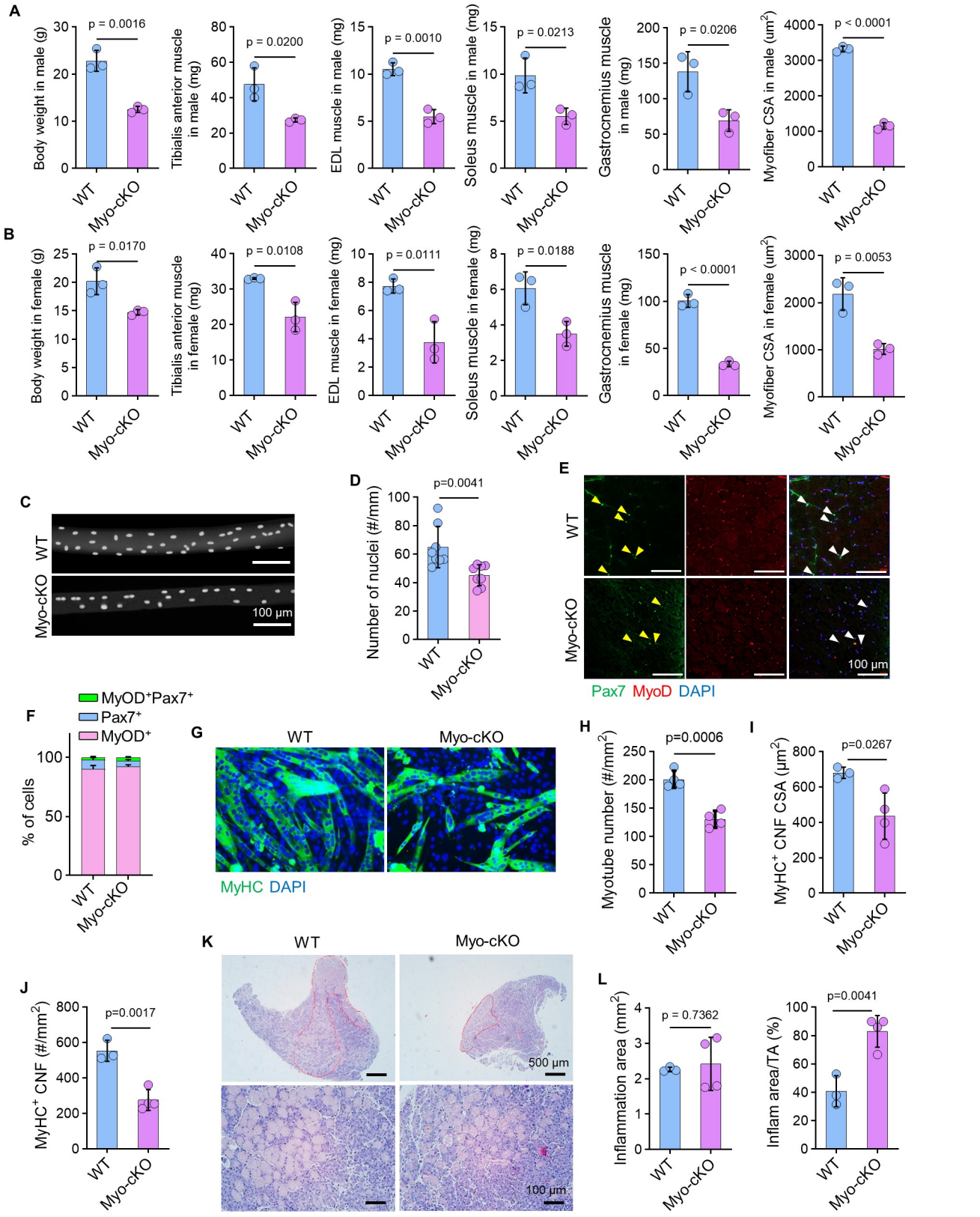

Supplementary Fig. 1. Myoblast-specific TRAF3 deficiency compromises muscle fiber maturation and regeneration. (A-B) Body weight, muscle mass and myofiber CSA in male (A) and female (B) MCK^{Cre}TRAF3$^{fl/fl}$ mice (refers to Myo-cKO) and TRAF3$^{fl/fl}$ (WT) littermates. n=3 mice/group. (C-D) Average number of nuclei on a single myofiber from Myo-cKO and WT mice. n=8 myofibers/group. (E-F) IF staining and quantification of Pax7-positive cells (MuSCs) and Pax7/MyoD double-positive cells (proliferating MuSCs) in TA muscle cross sections from the WT and Myo-cKO mice. (G-H) Myotube formation from primary myogenic cells (MCs; CD45$^-$CD11b$^-$CD31$^-$Sca1$^-$) isolated from skeletal muscles of 3-mon-old Myo-cKO and WT mice. n=4 mice/group. (I-J) CSA and number (per mm^2) of MyHC$^+$ CNFs in H&E-stained TA muscle sections. n=3 WT and 4 Myo-cKO mice. (K) H&E-stained TA cryosections (4 μm thick) of 3-mon-old WT and Myo-cKO mice injected with $BaCl_2$, and regions with no obvious damage or inflammatory cell infiltration outlined with red lines. (L) Inflammatory area and composition of this area in total TA CSA in H&E-stained TA muscle sections in (K). n=3 WT and 4 Myo-cKO mice. All data presented as mean ± SD. Analysis: Student's unpaired *t* test.

Supplementary Figure 2

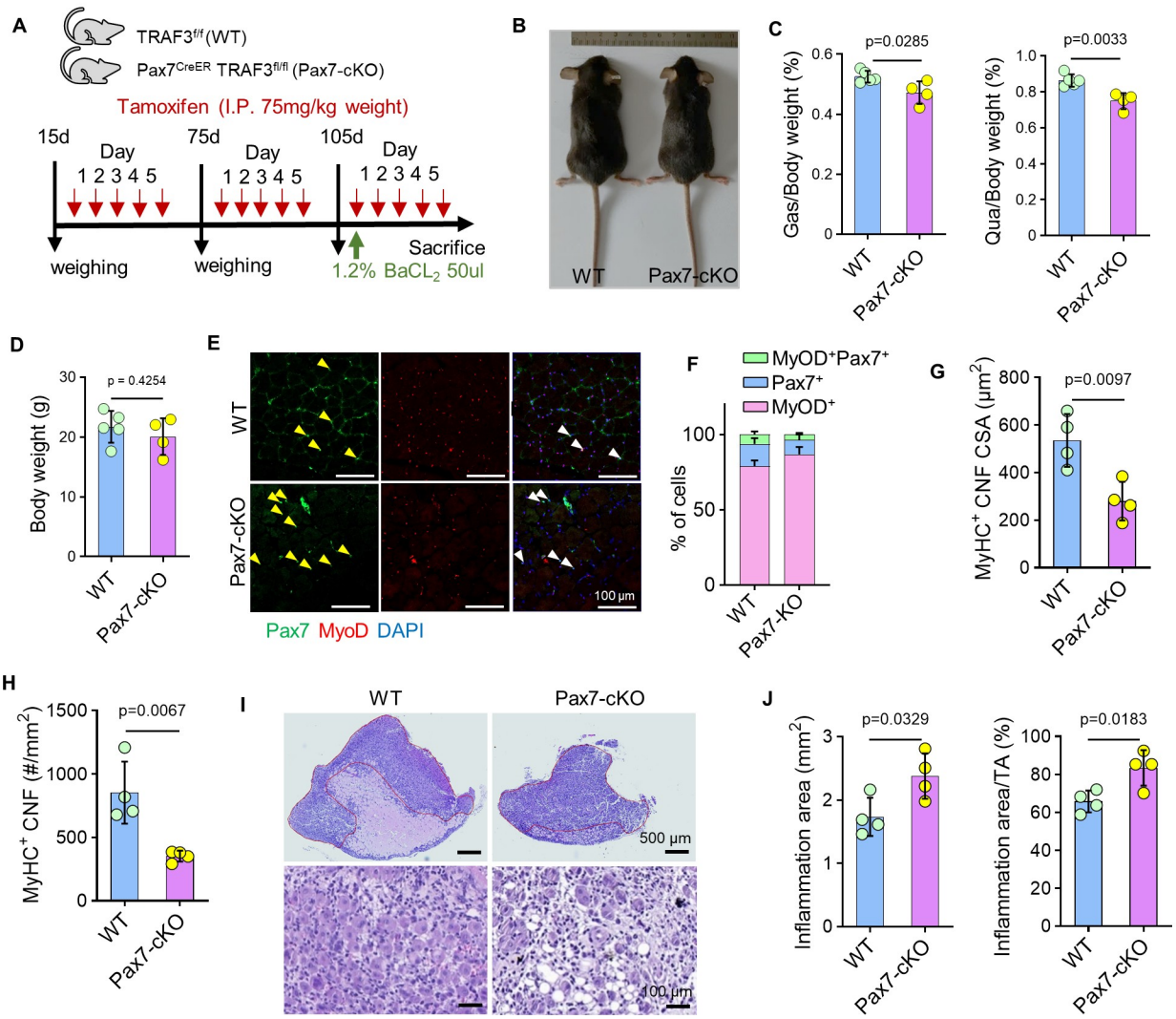

Supplementary Fig. 2. Satellite cell-specific TRAF3 deficiency compromises muscle fiber maturation and regeneration. (A) Experimental design of tamoxifen administration (I.P., 75 mg/kg body weight at age of 15, 75 and 105 days for total of 15 doses) in Pax7Cre^{ER}TRAF3$^{fl/fl}$ (refers to Pax7-cKO) mice and TRAF3$^{fl/fl}$ (refers to WT) mice. (B) Representative images of 4-mon-old Pax7-cKO and WT littermates, and (C) weights of gastrocnemius (Gas) and quadriceps (Qua) muscles, normalized to their respective body weights, from 4-mon-old Pax7-cKO and WT mice. n=5 WT and 4 Pax7-cKO mice. (D) Pax7-cKO and WT littermates body weights. n=5 WT and 4 Pax7-cKO mice. (E-F) IF staining and quantification of Pax7-positive cells (MuSCs) and Pax7/MyoD double-positive cells (proliferating MuSCs) in TA muscle cross sections from Pax7-cKO and WT mice. (G-H) CSA and number (per mm^2) of MyHC+ CNFs in H&E-stained TA muscle sections. n=4 mice/group. (I) H&E-stained TA cryosections (4 μm thick) of 3-mon-old WT and Pax7-cKO mice injected with $BaCl_2$, and the region with no obvious damage and inflammatory cell infiltration outlined using red lines. (J) Inflammation area and % of this area in total TA CSA in H&E-stained TA muscle sections in (I). n=4 mice/group. Analysis: Student's unpaired t test.

Supplementary Figure 3

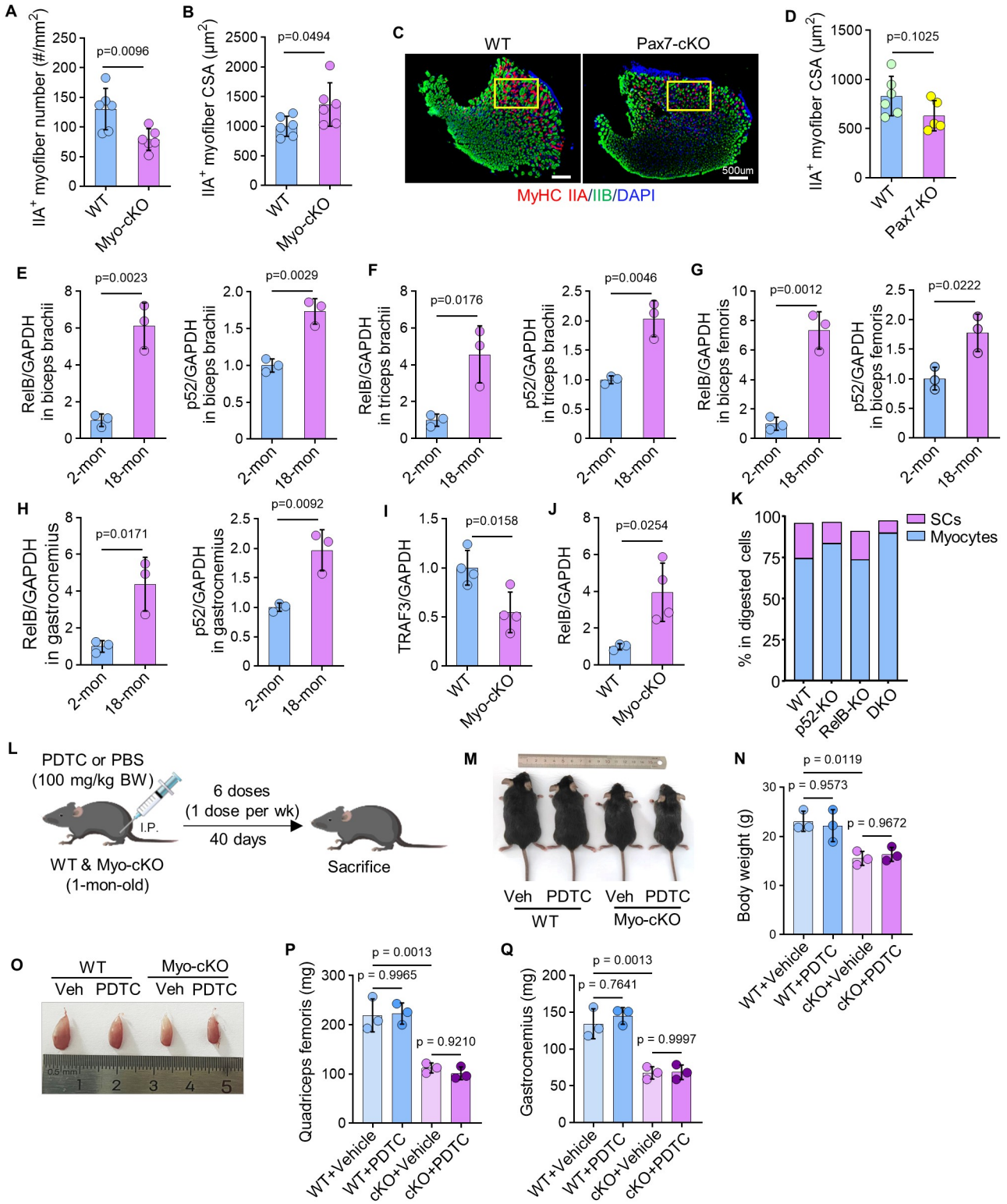

Supplementary Figure 3. Detrimental effects of TRAF3 on muscle homeostasis are largely independent of NF-κB activity. (A-B) CSA and number of MyHC IIA fibers from 3-mon-old Myo-cKO and WT mice. n=6 mice/group. (C) Representative images of IF staining for MyHC IIA (red) and IIB (green) in cryosections of TA muscles from 4-mon-old WT and Pax7-cKO mice, and (D) CSA of MyHC IIA fibers. n=6 WT and 5 Pax7-cKO mice. (E-H) RelB, p52 and GAPDH protein levels in biceps brachii, triceps brachii, biceps femoris and gastrocnemius muscles from young (2-mon-old) and old (18-mon-old) mice. n=3 mice/group. (I) TRAF3 and GAPDH protein levels in gastrocnemius muscles from Myo-cKO and WT mice tested by Western blot. n=4 mice/group. (J) RelB and GAPDH protein levels in gastrocnemius muscles from Myo-cKO and WT mice tested by Western blot. n=3 WT and 4 Myo-cKO mice. (K) % of SCs and myocytes in digested cells from p52 and RelB single- and double-knockout mice and WT mice. (L) Experimental design of PBS and PDTC administration (I.P., 100 mg/kg body weight for 40 d, 1 dose/1 wk) in 1-mon-old Myo-cKO and WT mice. (M-N) Representative images of vehicle- and PDTC-treated Myo-cKO and WT mice, and their body weights. n=3 mice/group. (O) Representative images of TA muscles from 3 vehicle- and PDTC-treated Myo-cKO and WT mice, and (P-Q) weights of quadriceps and gastrocnemius muscles, normalized to their respective body weights, n=3 mice/group. Analysis: Student's unpaired *t* test in (A-J), and one-way ANOVA with Tukey post analysis in (N-R).

Supplementary Figure 4

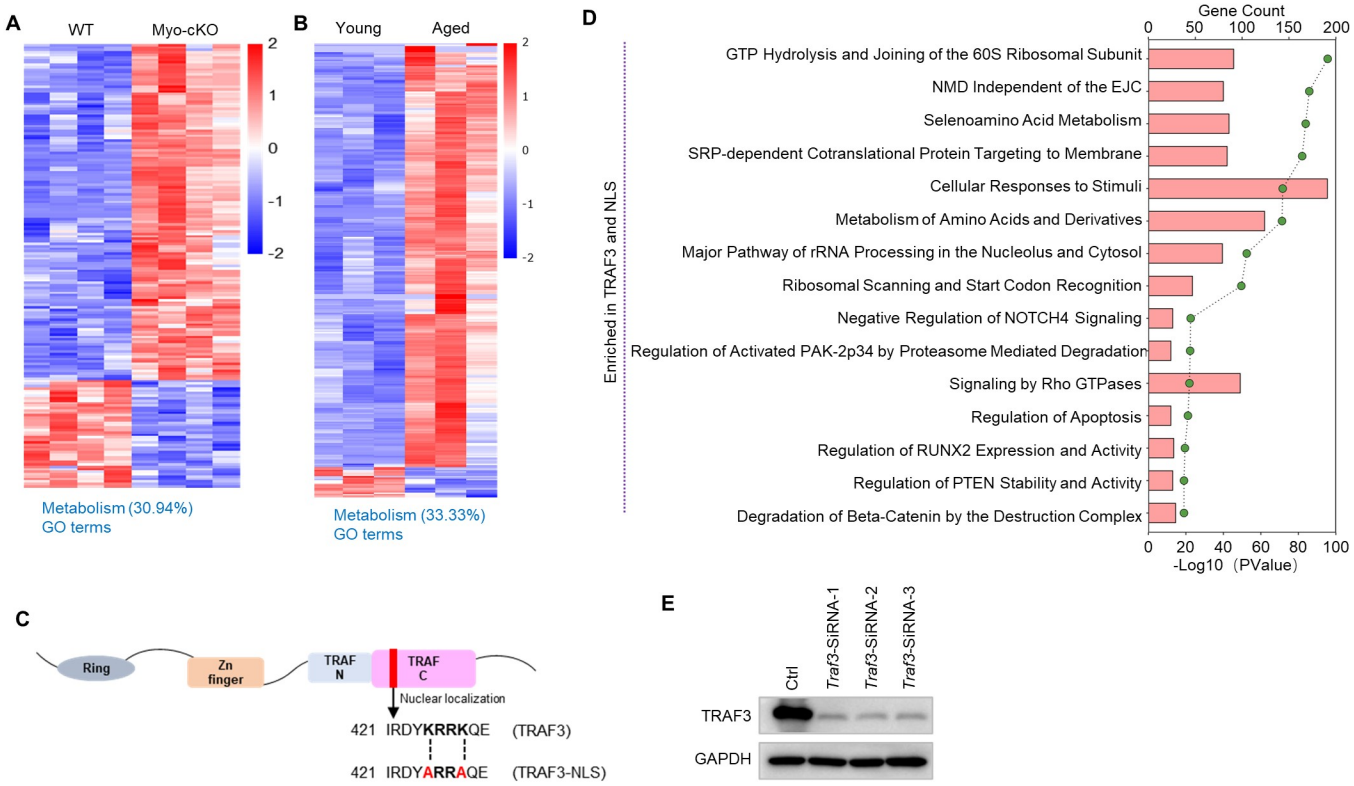

Supplementary Figure 4. **Direct binding of TRAF3 to ADSL facilitates metabolic processes in skeletal muscle.** (A-B) Heatmaps showing significantly changed genes in skeletal muscles from Myo-cKO mice and aged WT mice, compared to their respective controls. (C) Schematic showing the structure of full-length and NLS-mutated TRAF3. (D) Signaling pathways of enriched proteins binding to both full-length and NLS-mutated TRAF3. (E) Western blots of TRAF3 and GAPDH levels in C2C12 myoblasts treated with *Traf3* siRNA.

Supplementary Figure 5

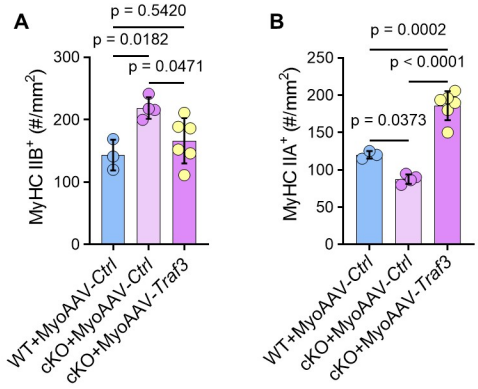

Supplementary Figure 5. TRAF3 restoration drives remodeling of skeletal muscle fibers. (A) Number of MyHC IIA and MyHC IIB fibers from MyoAAV-*Ctrl*-treated WT (n=3 mice) and Myo-cKO mice (n=4 mice), and MyoAAV-*Traf3*-treated M-cKO mice (n=6 mice). Analysis: one-way ANOVA with Tukey post analysis.

Supplementary Figure 6

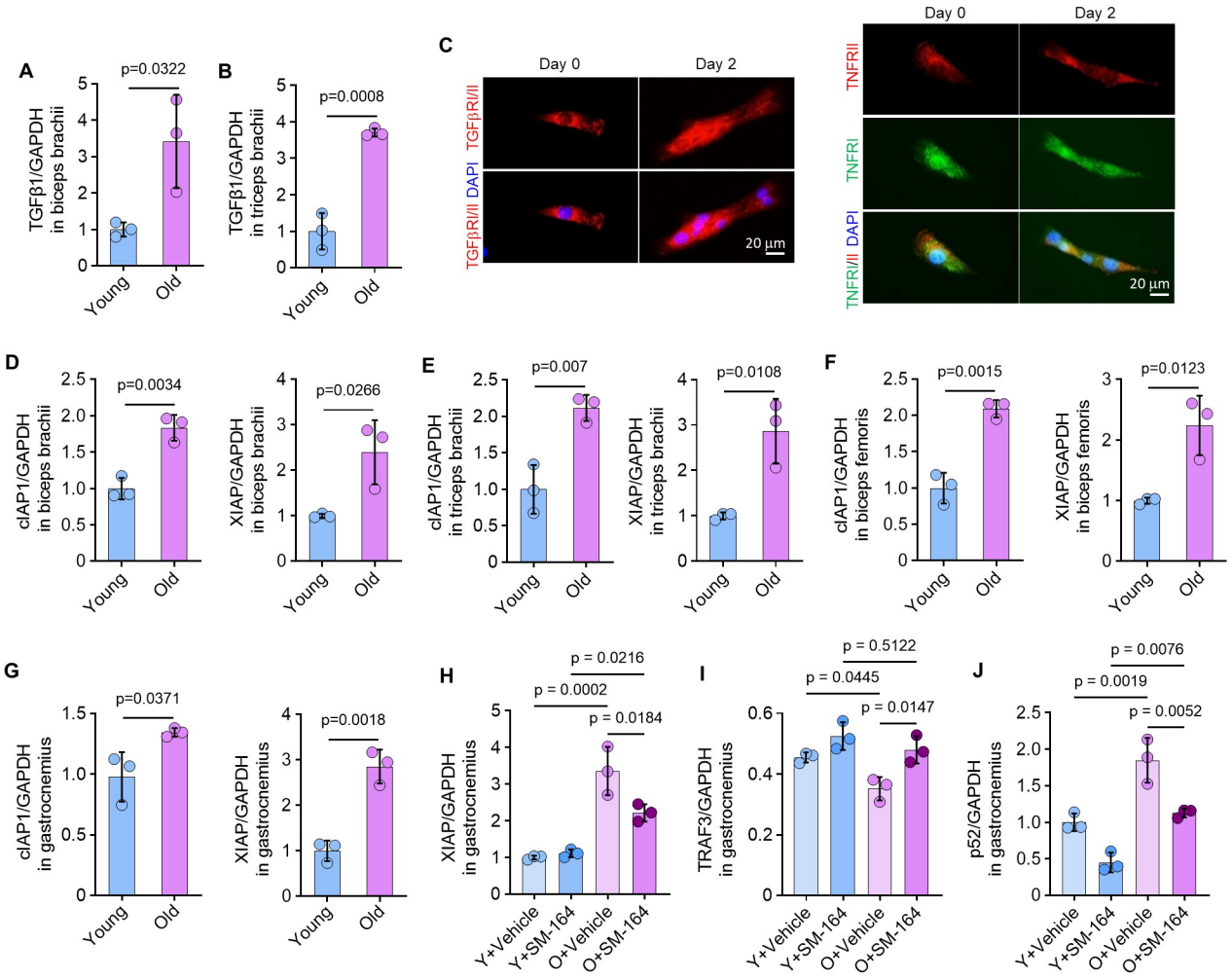

Supplementary Figure 6. TGFβ1 induces TRAF3 ubiquitination and degradation in skeletal muscle during aging. (A-B) TGFβ1 and GAPDH protein levels in biceps brachii and triceps brachii muscles from young (3-mon-old) and old (20-mon-old) mice. n=3 mice/group. (C) Representative images showing TNFR I and II , TGFβR I and II expression on cell membrane and cytoplasm of primary myocytes sorted from 22-mon-old C57 mice. (D-G) cIAP1, XIAP and GAPDH protein levels in biceps brachii, triceps brachii, biceps femoris and gastrocnemius muscles from young (2-mon-old) and old (18-mon-old) mice. n=3 mice/group. (H-J) XIAP, TRAF3, p52 and GAPDH protein levels in gastrocnemius from young (3-mon-old) and old (20-mon-old) mice treated with IAP inhibitor, SM164 (I.P., 3 mg/kg/d, once/d for 1 mon). Analysis: Student's unpaired *t* test in (A-G), and one-way ANOVA with Tukey post analysis in (H-J).

Supplementary Figure 7

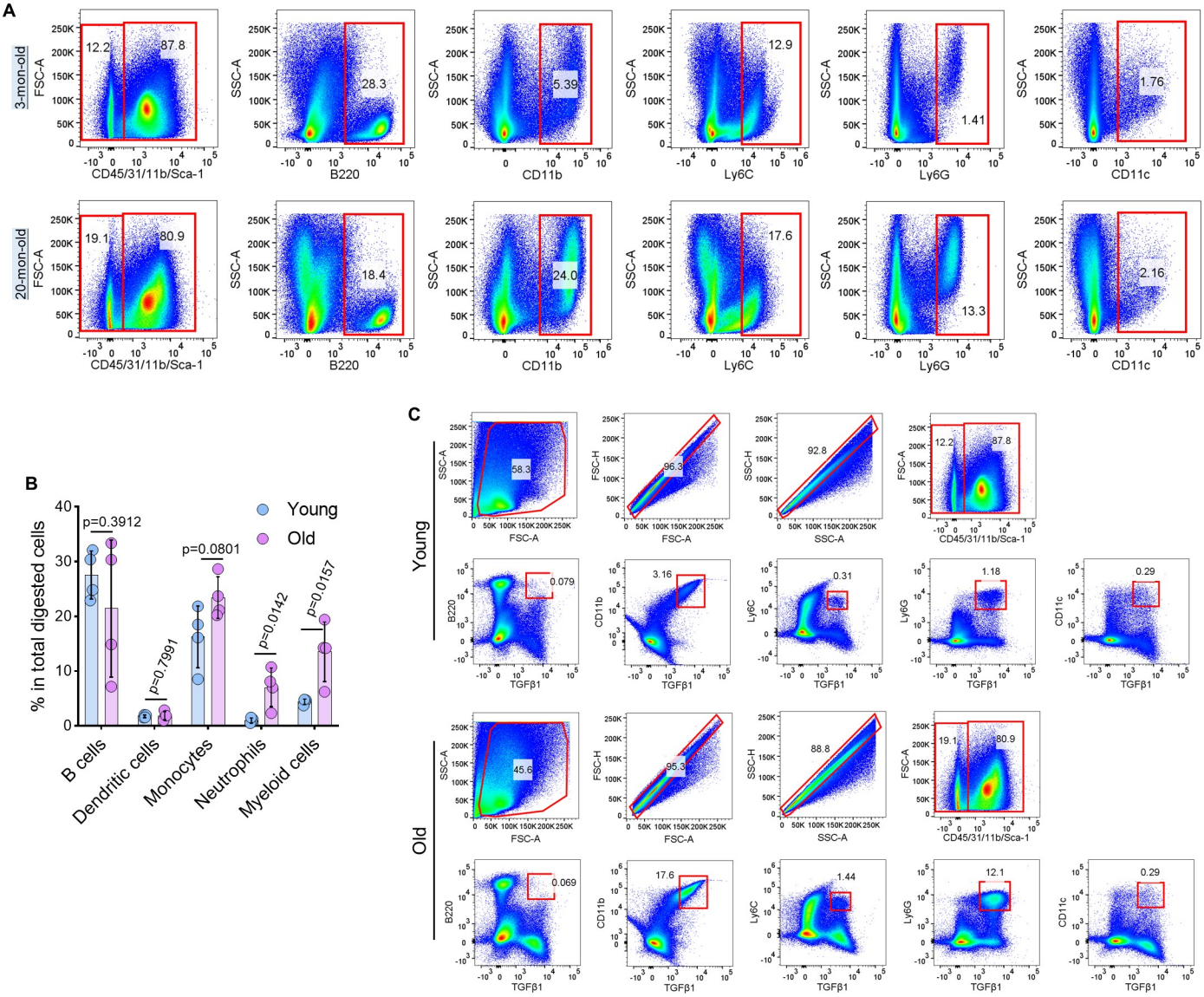

Supplementary Figure 7. Neutrophil-specific deletion of TGFβ1 drives changes in myofiber types in aged mice. (A) Gating strategy for myocytes and immune cells from skeletal muscles in young (3-mon-old) and old (20-mon-old) mice. (B) B cells ($B220^+$), dendritic cells ($CD11C^+$), monocytes ($Ly6C^+$), neutrophils ($Ly6G^+$) and myeloid cells ($CD11b^+$) from skeletal muscles in young (3-mon-old) and old (20-mon-old) mice. (C) Gating strategy for TGFβ1-expressing immune cells in cells digested from skeletal muscles of young (3-mon-old) and old (20-mon-old) C57 mice. Analysis: Student's unpaired *t* test.